https://doi.org/10.5194/esd-2021-75
Preprint. Discussion started: 20 October 2021


Earth System Dynamics Discussions

# Dominant influence of Pacific climate modes on global observed and reanalysis cloud cover fields

Petru Vaideanu[1,2], Mihai Dima[1,2], Monica Ionita[1,3] and Mirela Voiculescu[4]

[1]Alfred Wegener Institute Helmholtz Centre for Polar and Marine Research, Bremerhaven, 27570, Germany
[2]Faculty of Physics, University of Bucharest, Măgurele, 077125, Romania
[3] Emil Racovita Institute of Speleology, Romanian Academy, Cluj-Napoca, 400006, Romania
[4] Department of Chemistry, Physics and Environment, University "Dunărea de Jos", Galaţi, 800008, Romania

*Correspondence to*: Petru Vaideanu (petru.cosmin.vaideanu@awi.de)

**Abstract.** Global cloud cover represents a critical component of the climate system, with a considerable impact on the Earth's radiation budget. Small changes in clouds properties have a significant climatological impact because of the feedbacks that they generate, thus it is difficult to simulate the global cloud cover evolution in general circulation models. Observational investigations of cloud processes are constrained either by limited temporal and spatial extension of ground-based measurements or by imperfections in satellite data, like changes in geostationary satellite zenith angle, equatorial crossing time, or calibration. In this study, we used the Empirical Orthogonal Functions method to separate global patterns of total cloud cover variability in two satellite datasets from the International Satellite Cloud Climatology Project and the Pathfinder Atmospheres–Extended projects, each corrected for specific errors, and in the ERA5 Reanalysis. The first two modes explain most of the variance from what could be considered “signal” in both satellite data. Through Canonical Correlation Analysis, they are associated in a physically consistent manner with two different types of El Niño-Southern Oscillation (ENSO), namely the canonical ENSO which manifests itself in the eastern tropical Pacific and the El-Niño Modiki which manifest itself in the central Pacific. This work provides a comprehensive picture of the relationship between global total cloud cover and the tropical Pacific processes and indicates that cloud cover in the Indo-Pacific sector plays a significant role in the Earth radiative budget at interannual to decadal time scales. The similarity of the results across satellite and reanalysis data indicate that the both the observed and reanalysis cloud data sets contain consistent and valuable information related to global climate variability.

## 1 Introduction

Clouds have a complex influence on Earth’s radiation budget. Whereas high clouds tend to warm the surface by restricting the emission of longwave radiation emitted by Earth’s surface to space, low clouds tend to cool the surface by reflecting shortwave radiation coming from Sun, back to space (Ramanathan et al., 1989; Bony et al., 2004). Under these circumstances, predicting the behaviour of total cloud cover on a global scale is problematic and generates uncertainties in most climate projections (Cess et al., 1990; Dufresne and Bony, 2008; Zelinka et al., 2018), thus analysing observational cloud data is of great

https://doi.org/10.5194/esd-2021-75
Preprint. Discussion started: 20 October 2021


Earth System Dynamics Discussions

importance. Ground based data are restricted both at temporal and spatial scale, thus most recent studies of cloud cover rely on satellite data. However, these are also not perfect and issues affecting satellite cloud measurements are numerous, including biases from top-down viewing angles (Campbell and Holmlund, 2004), artificial trends connected to instrument degradation and orbital decay (Norris 2005), changes in the number of observing satellites (Evan et al., 2007), data intercalibration issues (Norris and Slingo, 2009), cloud overlap (Pallé, 2005) and biases connected to changes in viewing times and the diurnal cloud cycle (Jacobowitz et al., 2003).

Sea surface temperature (SST) and clouds are strongly linked through a variety of physical processes and feedbacks, making SST an important factor for cloud formation and behaviour (Ramanathan and Collins, 1991; Bony et al., 2015; Zhou et al., 2016). Furthermore, global climate sensitivity is essentially linked to Pacific SST and clouds variations (Silvers et al., 2017; Andrews and Webb, 2018). Previous studies linked changes in low cloud cover with the El-Niño-Southern Oscillation (Marsh and Svensmark, 2003) and with the Pacific Decadal Oscillation (Clement et al., 2009), whereas high cloud variations were associated with the 11-years solar cycle (Dima and Voiculescu, 2016) and with the Atlantic Multidecadal Oscillation (Vaideanu et al., 2017).

The El-Niño Southern Oscillation (ENSO) (Philander, 1990; McPhaden et al., 2006) is the most prominent mode of inter-annual variability in the climate system. Although significant progress has been made in understanding the dynamics and impact of the ENSO phenomenon, it's diversity and complexity is still a current and intriguing topic in the climate community (e.g.: Timmermann et al., 2018; Yeh et al., 2018). During the last decade, an increasing number of studies focused on two types of ENSO: 1) the conventional, canonical or Eastern Pacific (EP) ENSO, for which the maximum SST variability manifest in the eastern tropical Pacific (Rasmusson and Carpenter, 1982) and 2) the Central Pacific El-Niño (Yeh et al., 2009), known also as the El-Niño Modoki (Ashok et al., 2007), Warm Pool El-Niño (Kug et al., 2009), or date line El-Niño (Larkin and Harrison, 2005), with the maximum SST variability located over the central Pacific. In this study, we use the generic term CP ENSO to refer to the latter. It has been proposed that the EP-type and the CP-type of ENSO have distinct impacts on regional temperature, precipitation and storm track activity (Ashok et al., 2009; Feng and Li, 2011). The CP ENSO was observed to occur more frequently in recent decades, but its duration is shorter than that of the EP ENSO (Yu et al., 2010). This recent increase in the CP ENSO frequency, very likely higher than any other similar period over the last 400 years (Freund et al., 2019), was attributed to climate change (Yeh et al., 2009) and, as anthropogenic warming will intensify, it is argued that these events will become more frequent, in the detriment of the EP ENSO (Ashok and Yamagata, 2009; Timmermann et al., 2018).

The goal of this paper is to identify the dominant modes of total cloud cover variability on a global scale and to separate and quantify the impact of the EP ENSO and the CP ENSO on their evolution. This is achieved through multivariate statistical analysis based on two distinct sets of observational cloud data, each corrected for specific errors (Norris and Evan, 2015) and on latest reanalysis data from the European Centre for Medium-Range Weather Forecasts (ERA5R). Section 2 includes a description of the observational data and of the statistical methods used in this study. In the third section the main results of this study are presented. Discussions and conclusions are presented in section 4.

https://doi.org/10.5194/esd-2021-75
Preprint. Discussion started: 20 October 2021



## 2 Data and Methods

### 2.1 Data

Oscillatory modes in total cloud cover (TCC) are identified in two datasets of satellite measurements: i) The International Satellite Cloud Climatology Project (ISCCP) (Rossow et al., 1996; Rossow and Schiffer, 1999) and ii) the Pathfinder Atmospheres–Extended (PATMOS-x) fields (Heidinger et al., 2012; Heidinger et al., 2014). The ISCCP and PATMOS-x datasets have been used in many studies on causes and mechanisms of cloud changes (Zelinka and Hartmann, 2011; Klein et al., 2013). However, as with many retrieval fields, these datasets are accompanied by uncertainties. These are related to changes in geostationary satellite zenith angle (Evan et al., 2007), to low cloud cover masked by overlapping high clouds (Pallé, 2005), to changes in equatorial crossing time, (Jacobowitz et al., 2003; Heidinger et al., 2014) and to changes in calibration (Norris and Slingo, 2009). These artifacts in the ISCCP and PATMOS-x data have been addressed and corrected by Norris and Evan (2015), who produced an adjusted version for both TCC data. In this paper, we used these adjusted versions of the IPSCC and PATMOS-x TCC fields, distributed on a 2.5 º x 2.5 º global grid and extending over the 1984 –2009 period. The corrected versions of the ISCCP and PATMOS-x total coud cover data were obtained from the Research Data Archive at NCAR at https://rda.ucar.edu/datasets/ds741.5/ .

To compare the results obtained with the ISPCC and PATMOS-x satellite TCC data, we also make use the total cloud cover data from the fifth generation European Centre for Medium-Range Weather Forecasts (ECMWF) reanalysis (ERA5R) (Hersbach et al., 2020), extending over the 1979-2020 period. From the ERA5R we also used the sea level pressure (SLP) and 10m-wind global fields on a 1º x 1º resolution. The ERA5 Reanalysis project is the latest reanalysis from the ECMWF and provides a variety of atmospheric and climate variables. It uses state-of-the-art modelling and data assimilation system based on a large variety of historical observations of pressure, temperature, humidity and other variables (Hersbach et al., 2020). Compared to ERA-Interim, ERA5R has many improvements regarding parametrization and assimilation and could provide a more realistic representation of cloud physical processes (Hersbach et al., 2020). The ERA5R data are available at https://apps.ecmwf.int/data-catalogues/era5/?class=ea .

The sea surface temperature (SST) field is provided by the United Kingdom Met Office's (UKMO), through the Hadley Centre Sea Ice and Sea Surface Temperature dataset (HadISST) (Rayner et al., 2003), on grid with a 1º x 1º resolution, extending from 1870 to 2020. The variability of the global SST field is dominated by the spatially quasi-uniform warming trend which could mask the internal modes. Therefore, trends are removed in a preliminary stage, by subtracting from each grid point the annual global average. Interestingly, similar results are obtained if the warming trend is not removed from the global SST field. The HadISST data are available at https://www.metoffice.gov.uk/hadobs/hadisst/ .

For the observed total precipitation rate (TPR) field, we used the Combined Precipitation Data Set, provided by the Global Precipitation Climatology Project (GPCP) (Adler et al., 2003) distributed on a 1.5 º x 1.5 º grid, extending over the 1979 – 2020 period, available at https://psl.noaa.gov/data/gridded/data.gpcp.html .

https://doi.org/10.5194/esd-2021-75
Preprint. Discussion started: 20 October 2021


Earth System Dynamics Discussions

As a measure of the EP ENSO evolution, we used the Niño3 index. The Niño3 and the Niño4 time series are highly correlated ($r>0.8$). There is still no consensus about the proper index to describe CP ENSO evolution (Ashok et al., 2007; Ren and Jin, 2011; Jeong and Ahn, 2017). In this study, we used the Trans-Niño Index (TNI), which is defined as the difference of the normalized SST anomalies from the Niño 4 and the Niño 1+ Niño 2 regions (Trenberth and Stepaniak, 2001). The low correlation between TNI and the Niño3 Index ($r<0.15$) supports the idea that these two-time series are describing distinct evolutions of these two types of ENSO-like events. The Niño3 Index, and the TNI Index are obtained from http://www.esrl.noaa.gov/psd/data/climateindices/list/ . For all datasets, monthly anomalies from the annual cycle are calculated and then annual means are computed.

### 2.2 Methods

The dominant modes of TCC are derived by using the Empirical Orthogonal Functions (EOF) method (Lorenz, 1956). This technique uses an orthogonal transformation to transform a set of observations of correlated variables into a set of values of non-correlated linear variables. The uncorrelated variables represent linear combinations of the initial ones. The first main component explains the maximum amount of the variance from the original variables; the second one explains the maximum amount of the remaining variance, not explained by the first component, and so on. As it is essentially based on pattern separation, the EOF analysis is an efficient method to investigate the spatial and temporal variability of time series, extending over relatively large areas.

To identify the coupled cloud cover and the global SST patterns, we employed Canonical Correlation Analysis (CCA) (von Storch and Zwiers, 1999). The CCA is a powerful multivariate technique used to identify pairs of patterns with maximum correlation between their associated time series. In other words, CCA determines the extent to which two phenomena, each described by a variable or a set of variables, are linked. Mathematically, CCA transforms pairs of originally centered vectors $X_0$ and $Y_0$ into sets of new variables, called canonical variables. The canonical correlations are determined by solving the eigenvalue equations:

$$\begin{cases} [C_{xx}]^{-1}[C_{xy}][C_{yy}]^{-1}[C_{yx}]\,W_x = \rho^2 W_x \\ [C_{yy}]^{-1}[C_{yx}][C_{xx}]^{-1}[C_{xy}]\,W_y = \rho^2 W_y \end{cases} \quad (1)$$

Where: $C_{xx}$ and $C_{yy}$ are the matrices of covariance for x and y respectively,

$C_{xy}=C^{-1}{}_{yx}$ is the between-sets covariance matrix,

$\rho^2$ eigenvalues are the squared canonical correlations, and the eigenvectors,

$W_x$ and $W_y$ are the normalized canonical correlation basis vectors.

As the core constraint of the method is the maximization of correlation between time components, the corresponding patterns are provided by the method even if they do not explain a large amount of the variance in their fields, which means that the patterns explaining largest percent of variance do not necessarily appear in the first pairs.

https://doi.org/10.5194/esd-2021-75
Preprint. Discussion started: 20 October 2021


Earth System Dynamics Discussions

The statistical significance of correlations and regressions are examined in relation to the (two-tailed) probability (p) value to obtain a similar correlation value by chance. Because the significance is affected by the autocorrelation of each time series, the effective number of degrees of freedom used to calculate is computed with the relation): $Nef = N (1 - R_1R_2)/ (1 + R_1R_2)$, in which N is the number of values of the time series and $R_1$, $R_2$ represent the lag-one autocorrelation of each record (Bretherton et al., 1999).

### 2.3 Strategy

Generally, the EOF allows us to reduce the size of the data for a compact and optimal description of them, thus increasing the signal to noise ratio. However, it does not provide information about a specific forcing since a mode could be influenced by several different forcing factors. Unlike EOF, which is based on the distinction between patterns (they are orthogonal), CCA is based on the distinction between time evolution of patterns (the time series of consecutive pairs are uncorrelated). Therefore, CCA can be used to determine the footprint of a forcing factor on a given field when distinct forcing factors are characterized by different temporal evolutions. The distinction between the TCC spatial structures associated with the EP ENSO and the CP ENSO in pairs derived through CCA is emphasized based on their specific SST footprint and also on their specific temporal evolution. The final assessment of the significance of the identified coupled patterns relies on their physical consistency. In order to validate the results across different statistical methods and to infer the physical relevance of the identified coupled patterns, the SLP, 10m-Wind and TPR fields are regressed on the time series of the associated pairs resulted from the CCA.
The observed TCC data include all physical processes involved in cloud formation. However, they are accompanied by different types of uncertainties and have been corrected trough different methods. The reanalysis data are less sensitive to measuring errors, but their accuracy is limited by model imperfections and by the finite number of processes considered in the numerical simulations. Thus, using two sets of satellite cloud data, each corrected for specific errors, together with data from state of the art ERA5 Reanalysis, we attempt to identify the biases associated with observational cloud data, on one hand, and to assess the accuracy of the ERA5R TCC data, on the other hand.

## 3 Results

### 3.1 Dominant modes of global total cloud cover variability

The first two modes of TCC variability, derived through the EOF analysis of the annual TCC anomalies from ISCCP, PATMOS-x datasets extending over the 1984–2009 period, and ERA5 Reanalysis over the 1979–2020 period, are shown in Fig. 1.
The spatial structures of EOF1, identified in ISCCP (Fig. 1a), PATMOS-x (Fig. 1c) and ERA5 (Fig. 1e), are qualitatively and quantitatively similar over most of the globe. They have the highest loadings in the tropical Pacific and can be characterized by a band of positive TCC anomalies extending from the west coast of Peru toward the central Pacific and negative loadings in the Central, North East and South East Pacific. They also include positive anomalies over most of the North America,

https://doi.org/10.5194/esd-2021-75
Preprint. Discussion started: 20 October 2021


Earth System Dynamics
Discussions
Open Access
EGU

Central Asia and the North Atlantic, more prominent in the ERA5 pattern (Fig. 1e) and less intense in the PATMOS-x data (Fig. 1c), but also negative values over the tropical Atlantic, extending over the north-eastern part of South America. Differences between the observed and reanalysis EOF1 patterns are noted over parts of Australia, north western part of South America and the South Atlantic. The three associated time series (PC1, Fig. 1g) are dominated by interannual variability and
165 are highly correlated (r ~0.9, significant at the 99% level).

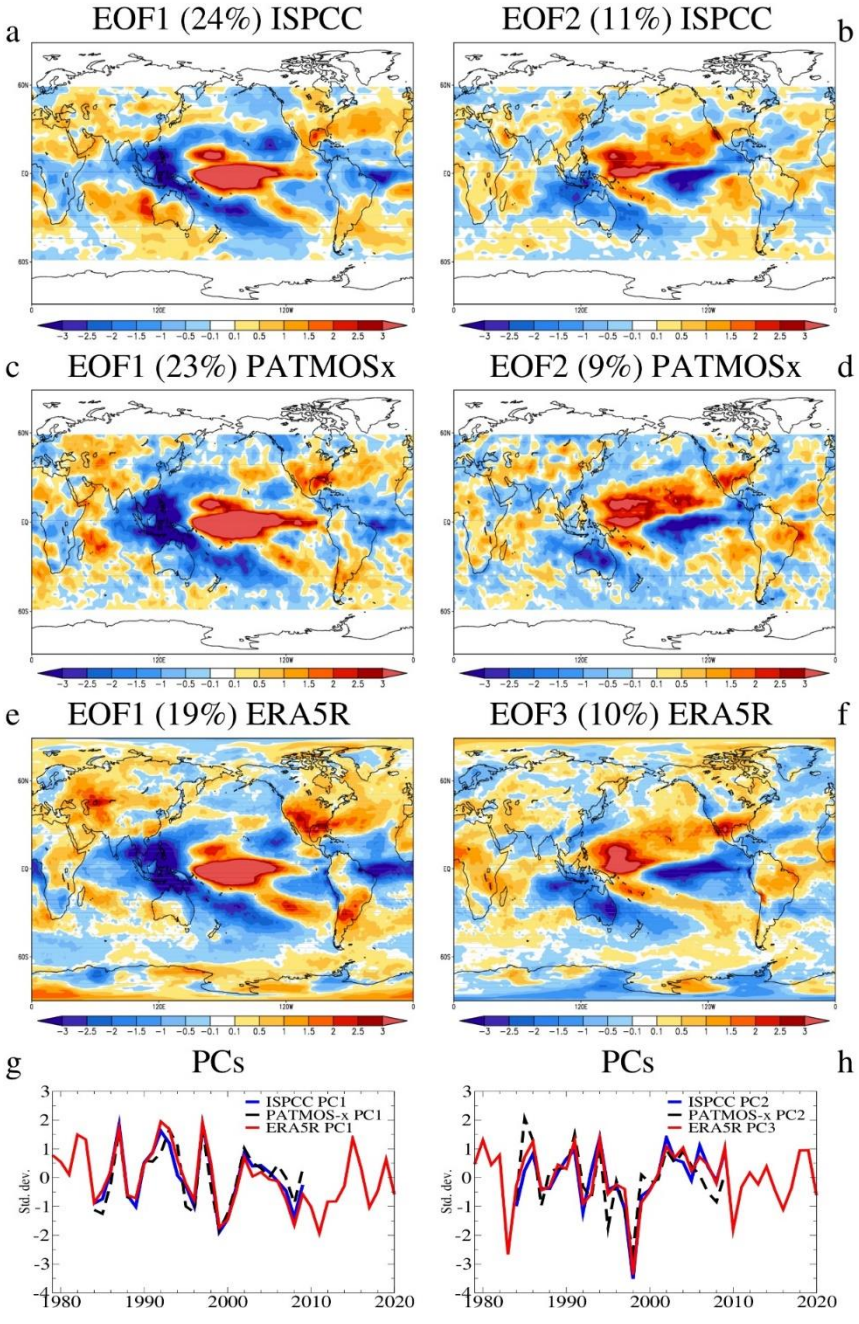

https://doi.org/10.5194/esd-2021-75
Preprint. Discussion started: 20 October 2021


Earth System Dynamics Discussions

**Figure 1:** Global modes of total cloud cover variability in observations and ERA5 Reanalysis data
Left column: The spatial structure of the dominant mode (EOF1) of TCC variability (%) based on ISCCP (a), PATMOS-x (c) and ERA5 Reanalysis (e) data with their associated time series (g). Right column: The second empirical orthogonal function (EOF2) of TCC variability (%) based on ISCCP (b) and PATMOS-x (d) data and the third EOF from ERA5 Reanalysis (f) data, with their associated time series (h).

The spatial pattern of the second EOF derived using the ISCCP (Fig. 1b) and the PATMOS-x (Fig. 1d) TCC data, and the third EOF from ERA5 (Fig. 1f), are similar over most of the globe, being characterized by an equatorial dipole of TCC anomalies in the equatorial Pacific, with intense positive loadings in the central part and negative anomalies in the eastern sector. They also include an increase in cloudiness in the north-eastern part of South America extending in the Tropical Atlantic, and a decrease in cloudiness over most of the North Atlantic. The associated PCs (Fig. 1h) have no increasing trend and their correlation coefficient is ~ 0.77 (significant at the 99% level). The second EOF derived using the ERA5R TCC data (Supp. Fig. 1) is not of interest for our study due to its temporal characteristics.

The maximum TCC positive anomalies of spatial structures for both EOFs are located in the Tropical Pacific, and their PCs are dominated by interannual variability. The combined variance explained by the first two modes, is 35 % in ISCCP (Fig.1a and b), 32 % in the PATMOS-x fields (Fig. 1c, 1d). A large part of the distribution of the rest of the observed EOFs variance (about 55%), is quasi-equally shared by a large number of modes, each explaining less than 5% of variance (Supp. Table 1), which suggests that these are associated with noise. Therefore, the first two modes identified in satellite observations explain two thirds from the approximately 45% of variance which can be considered "signal" in both satellite cloud data.

### 3.2 Observed coupled SST-TCC patterns associated to interannual Pacific climate variability

In order to identify global observed SST-TCC pairs, two CCAs were performed for 1984 – 2009 using the observed SST: one using corrected TCC anomalies from ISPCC data and the other using TCC data from PATMOS-x. The results shown in Fig. 2 (for ISCCP) and Fig. 3 (for PATMOS-x), respectively and are summarized in Table 1.

**Table 1:** The variances explained by the EP ENSO and the CP ENSO SST/TCC patterns from ISPCC (Fig.2), PATMOS-x (Fig.3) satellite observations and ERA5 Reanalysis (Fig.4).

| CCA | Explained variance (SST) | Explained variance (TCC) | Correlation coefficient PCs | Footprint | Correlation with the associated index | Projection on EOF1 1 = identical projection | Projection on EOF2 1 = identical projection | Projection on decadal variability max value = 1 |
|---|---|---|---|---|---|---|---|---|
| *ISPCC* 3rd pair | 20 % | 22 % | 0.98 | EP ENSO | 0.84 | **0.94** | 0.03 | 0.35 |
| *ISPCC* 4th pair | 7% | 7% | 0.97 | CP ENSO | 0.67 | 0.04 | **0.89** | 0.26 |
| *PATMOS-x* 3rd pair | 16% | 17% | 0.99 | EP ENSO | 0.8 | **0.79** | 0.02 | 0.29 |

https://doi.org/10.5194/esd-2021-75
Preprint. Discussion started: 20 October 2021


Earth System Dynamics Discussions

| | | | | | | | | |
|---|---|---|---|---|---|---|---|---|
| *PATMOS-x* 4th pair | 9% | 8% | 0.98 | CP ENSO | 0.73 | 0.01 | **0.71** | 0.21 |
| *ERA5* 3rd pair | 16% | 13% | 0.98 | EP ENSO | 0.91 | **0.95** | 0.02 | 0.25 |
| *ERA5* 5th pair | 7% | 7% | 0.97 | CP ENSO | 0.72 | 0.06 | **0.81** | 0.17 |

The spatial structures of the first two pairs identified through the two CCAs explain less than 6% of variance (Supp. Table 2) and are not of interest in our study. This is not totally unexpected, since the CCA method ordinates the pairs based on the correlation between the temporal evolutions of the associated spatial structures and not based on the percentage of explained variance.

The third and fourth coupled SST-TCC pairs, derived through CCA using the ISPCC TCC fields are shown in Fig. 2. The SST spatial structure of the third pair, (Fig. 2a) explains 20%/ of the total variance and is dominated by a band of positive anomalies located in the eastern tropical Pacific, surrounded by negative values, which is a typical structure for the positive phase of the EP-ENSO (e.g. Philander, 1990; Ashok and Yamagata, 2009). The associated TCC pattern (Fig. 2e) is characterized by positive anomalies in the eastern-central Pacific and over the North and the South Atlantic, and negative anomalies in the western-central Pacific, the north-east (NE) and the south-east (SE) Pacific. The TCC spatial structure explains 22% of the total cloud cover variance and projects strongly on EOF1 (Fig. 1a) (projection coefficient of 0,94, where r =1 is the maximum value and represents identical projection) (see Table 1). The corresponding time series (Fig. 2c) are dominated by inter-annual variability are significantly correlated with the Niño3 Index (r=0.84) and have the maximum amplitude in 1997-1998, when a strong EP ENSO event was recorded (Yu and Kim, 2013). The SST structure of the fourth pair (Fig. 2b) explains 7% of the total variance and can be described by the following features: i) the highest positive values are located in the central tropical Pacific; ii) a horizontal V-shaped anomaly structure with positive values, starting from the central tropical Pacific and extending toward the subtropics in both hemispheres; iii) negative SST anomalies near the northwest coast of South America. These characteristics were identified as the SST signature of CP ENSO in previous observational and numerical studies (Ashok et al., 2007; Ashok and Yamagata, 2009; Kao and Yu, 2009; Yeh et al., 2009; Yu et al., 2010). The associated TCC spatial structure (Fig. 2f) has the highest loadings in the central Pacific, with positive values in the central tropical Pacific and negative TCC anomalies in the eastern tropical Pacific, surrounded by positive TCC values in the subtropics. This feature is significantly distinct from any characteristic associated with the EP ENSO (Fig. 2e). The TCC spatial structure explains 7% of the total variance and projects strongly on EOF2 (Fig. 1b) (r =0,76, where r =1 is the maximum value and represents identical projection). The association of the TCC structure with CP ENSO is supported also by the associated PC-s of this pair (Fig. 2d) which are significantly correlated (r=0.67, significance level >95%) with the TNI Index, which is a very good measure for CP ENSO events (Trenberth and Stepaniak, 2001).

https://doi.org/10.5194/esd-2021-75
Preprint. Discussion started: 20 October 2021


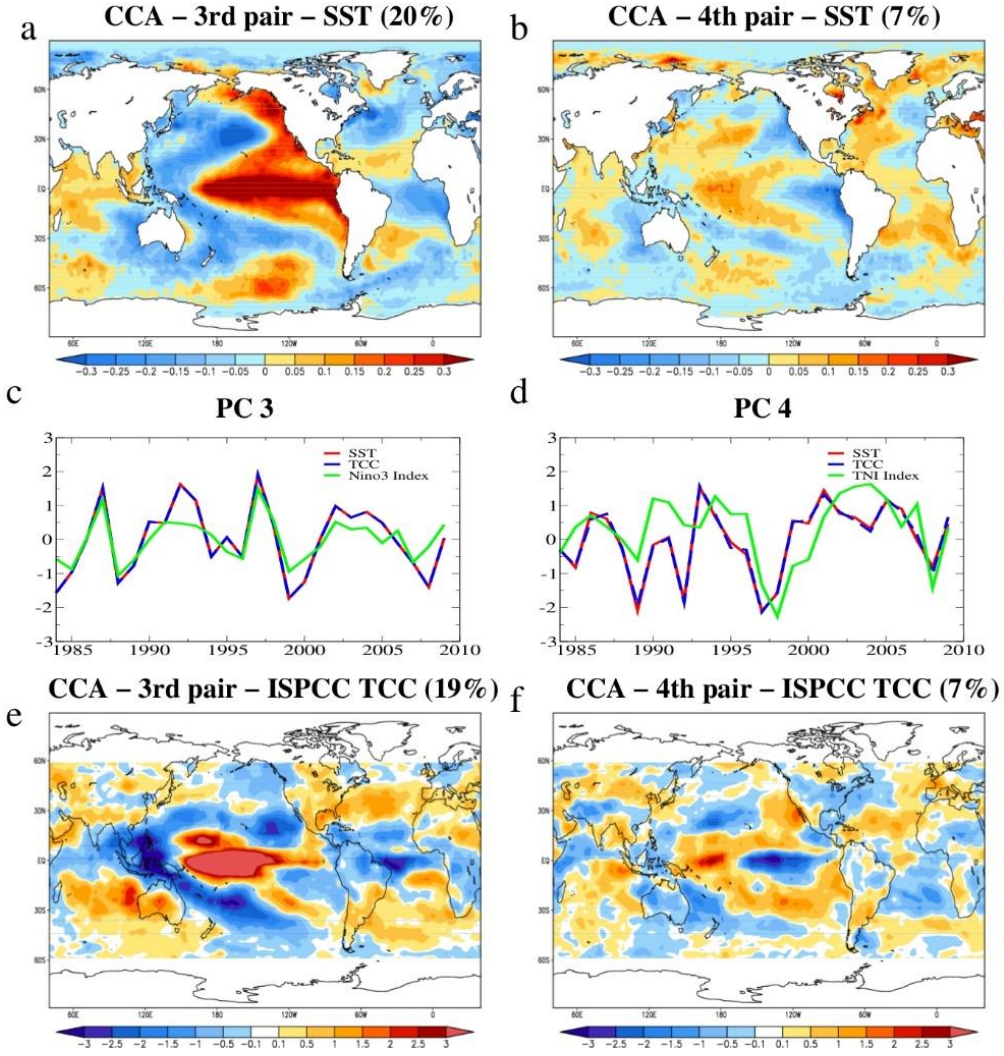


**Figure 2:** The EP ENSO (left) and the CP ENSO (right) footprints on global SST-TCC fields identified through CCA using ISPCC total cloud cover data extending over 1984 – 2009 period. Left column: The third coupled SST (°C) - TCC (%) pair: the SST pattern (a), explaining 20 % of variance, the TCC structure (e), explaining 19 % and the associated time series (c) with TCC (blue line), SST (red line). The corelation with the Nino3 Index (green line) is 0.81 Right column: The forth coupled SST (°C) - TCC (%) pair: the TCC pattern (a), explaining 7 % of variance, the SST structure (c), explaining 7 % and the associated time series (e) with TCC (blue line), SST (red line). The corelation with the TNI Index (green line) is 0.61.

A similar CCA was performed using the PATMOS-x total cloud cover data (Fig. 3). The ISPCC and the PATMOS-x satellite data, each have specific errors which have been corrected trough different techniques (Norris and Evan, 2015). Therefore, it is

https://doi.org/10.5194/esd-2021-75
Preprint. Discussion started: 20 October 2021


Earth System Dynamics Discussions
Open Access
EGU

very likely that common features captured in both of them reflect real phenomena and are not the effect of imperfections and possible biases existent in satellite cloud data. The associated temperature (cloud) pattern of the third SST-TCC (PATMOS-x) pair explains 16% (17%) of the total variance, whereas temperature (cloud) spatial structure of the fourth pair explains 9% (8%) of the total variance (Table 1). The SST pattern of the third pair (Fig. 3a) is characteristic for the EP ENSO, with intense positive SST's in the Eastern tropical Pacific. The corresponding time series (Fig. 3c) follow closely the Niño3 index (r=0,8, significance level >95%). The associated TCC structure (Fig. 3e) includes positive anomalies in the eastern tropical Pacific, in the North Atlantic and over most of the North America, and intense negative anomalies in the central-western Pacific, similar with the EP ENSO footprint obtained using the ISPCC data (Fig. 2e). Differences between the two observed TCC spatial structures associated to the EP ENSO are observed over Australia, parts of South America and Africa.

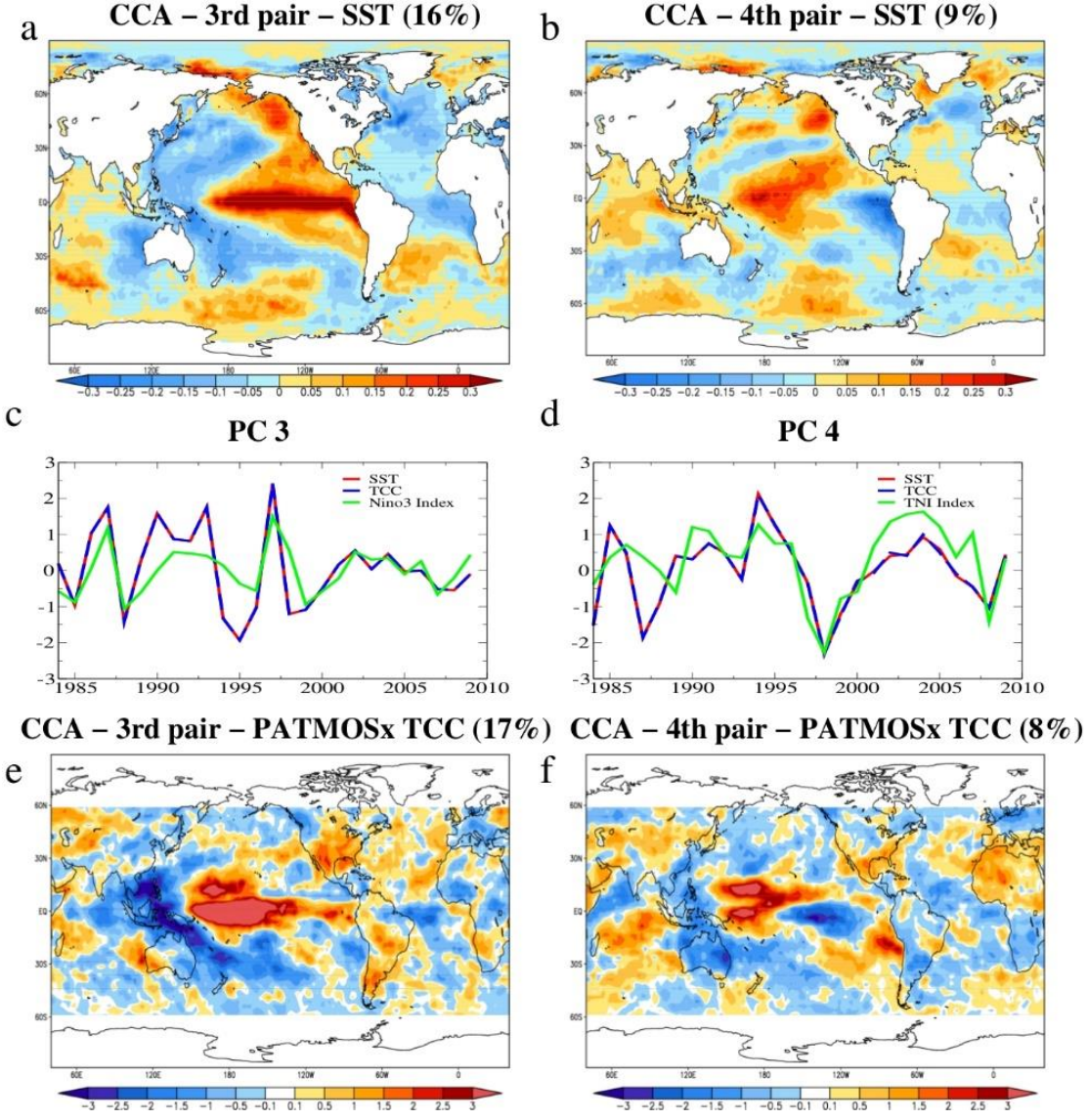

https://doi.org/10.5194/esd-2021-75
Preprint. Discussion started: 20 October 2021


Earth System Dynamics Discussions

**Figure 3***:* The EP ENSO (left) and the CP ENSO (right) footprints on global SST-TCC fileds identified through CCA using PATMOS-x total cloud cover data extending over 1984 – 2009 period. Left column: The third most coupled SST (°C) - TCC (%) pair: the SST pattern (a), explaining 16% of variance, the TCC structure (e), explaining 17% and the associated time series (c) with TCC (blue line), SST (red line). The corelation with the Nino3 Index (green line) is 0.79. Right column: The fourth most coupled SST (°C) - TCC (%) pair: the TCC pattern (b), explaining 9% of variance, the SST structure (f), explaining 8% and the associated time series (d) with TCC (blue line), SST (red line). The corelation with the TNI Index (green line) is 0.73.

The SST and the TCC spatial structures of the fourth pair (Fig. 3b and f) can be characterized by an east-west dipole of SST/TCC anomalies located in the tropical Pacific, with positive values in the central Pacific and negative loadings in east, more prominent than in the CP ENSO pair obtained using the ISPCC data (Fig. 2b and f). Their associated time series (Fig. 3d) have a correlation coefficient of 0.73 (significant over 95 % confidence level) with the TNI Index further supporting the association of this pair with the CP ENSO.

Both the ISCCP and the PATMO-x datasets capture the main features of the EP ENSO and the CP ENSO modes over the oceans, but the results obtained using the PATMOS-x data are more consistent with previous regional studies over the North America (Chiodi and Harrison, 2013), the South America (Garreaud et al., 2009) and Australia (King et al., 2015), indicating that this dataset is more suitable for regional investigations regarding the ENSO (Supp. Fig. 2). Together, the two global TCC spatial patterns explain more than 25 % of the global cloud cover variance or ~ 60% of the "signal", considering the level of noise in both TCC datasets (Supp. Table 2). In the tropical Pacific, a positive correlation between SST and TCC anomalies is observed in all analysed pairs while in the NE and the SE Pacific, a negative SST-TCC correlation is observed, more prominent in the results obtained using the ISPCC fields. Both TCC patters associated with the CP ENSO (Fig. 2e and Fig. 3e) project strongly on EOF1, while the TCC spatial structures associated with the CP ENSO (Fig. 2f and Fig. 3f) project strongly on EOF2 (Table 1), indicating that the two ENSO modes dominate the evolution of global total cloud cover variability.

### 3.3 Coupled SST- Reanalysis TCC patterns associated to interannual Pacific climate variability

In order to test the robustness of the results on a different time frame, we performed also a CCA using the ERA5 Reanalysis total cloud cover data, extending over the 1979–2020 period, with the results shown in Fig.4.

The SST spatial structure of the 3$^{rd}$ pair (Fig. 4a) explains 16% of variance and resembles the EP ENSO, with a band of intense positive SSTs in the Eastern tropical Pacific, flanked by negative loadings, positively correlated with the associated TCC structures. The reanalysis TCC spatial structure associated to the EP ENSO (Fig. 4e) includes positive loadings in the eastern tropical pacific, over most of North America and the North Atlantic, while negative anomalies are present over the western Pacific, over the NE and the SE Pacific, and over the tropical Atlantic. The reanalysis EP ENSO TCC footprint is quantitative and qualitative similar over most of the globe with both the ISPCC (Fig. 2e) and PATMOS-x (Fig. 3e) footprints but resembles more the one obtained using ISPCC data over the continents. The associated time series (Fig. 4e) are significantly correlated with the Niño3 Index (r=0.91. >95% significance level). The SST structure of the 5$^{th}$ coupled pair (Fig. 4d) is dominated by a

https://doi.org/10.5194/esd-2021-75
Preprint. Discussion started: 20 October 2021


Earth System Dynamics Discussions
Open Access
EGU

dipole of anomalies in the Atlantic basin, with intense positive loadings in the Central Pacific, a structure typical for the CP ENSO. The coupled TCC pattern include negative anomalies in the Eastern tropical Pacific and positive anomalies in the Central Pacific, in very good agreement with the TCC pattern associated to the CP ENSO using the ISPCC (Fig. 2f) and PATMOS-x (Fig. 3f) data. The time series associated to the coupled patterns (Fig. 4f) are significantly correlated with the TNI index (r=0.72, >95% significance level).

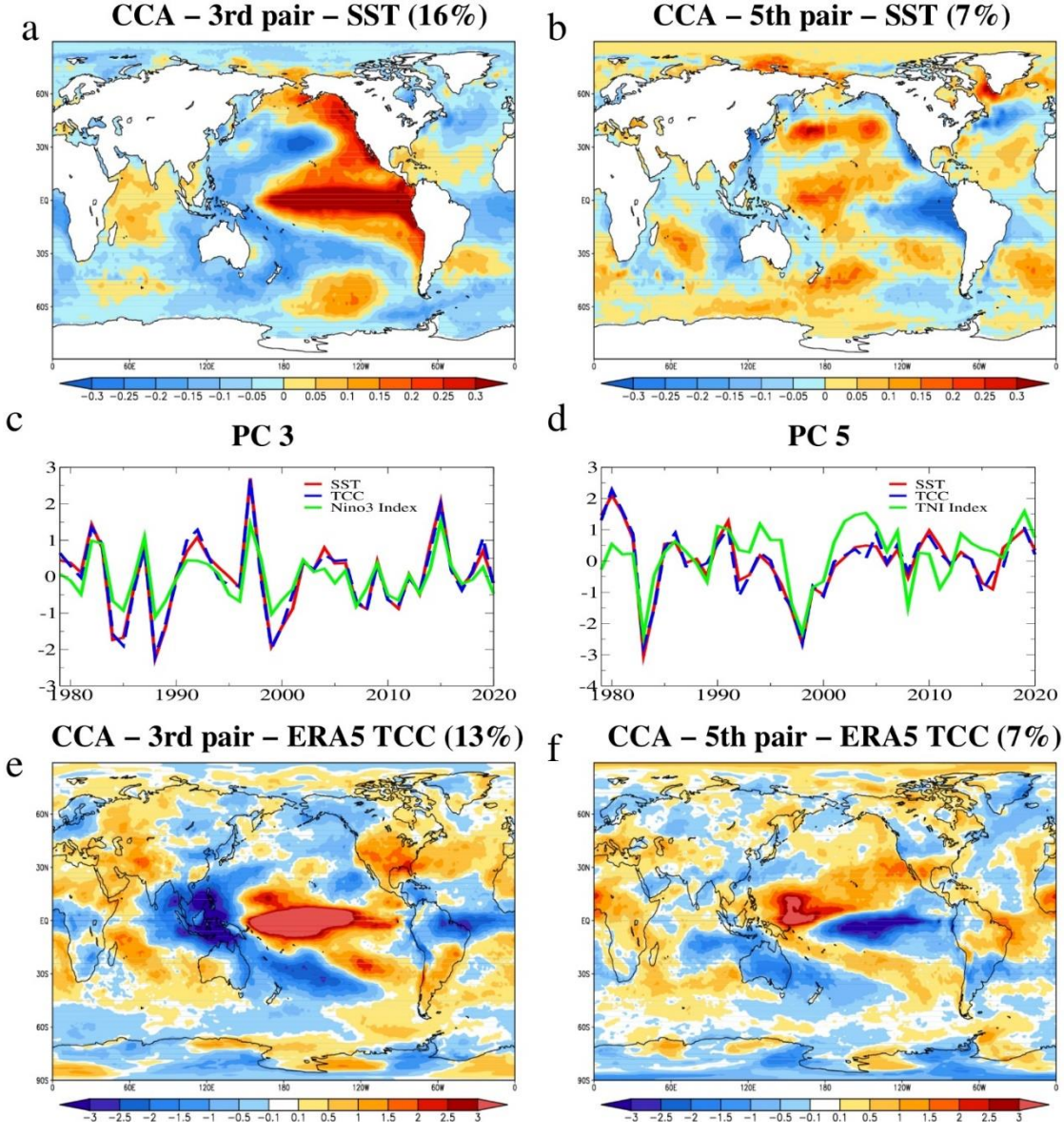

https://doi.org/10.5194/esd-2021-75
Preprint. Discussion started: 20 October 2021


Earth System Dynamics Discussions

**Figure 4:** The EP ENSO (left) and the CP ENSO (right) footprints on global SST-TCC fields identified through CCA using ERA5 total cloud cover data extending over the 1979 - 2020 period. Left column: The third most coupled TCC SST (°C) - TCC (%) pair identified through CCA using ERA5 TCC data: the TCC pattern (a), explaining 16 % of variance, the SST structure (c), explaining 13 % and the associated time series (e) with TCC (blue line), SST (red line). The corelation with the Nino3 Index (green line) is 0.89. Right column: The fifth most coupled SST (°C) - TCC (%) pair: the TCC pattern (b), explaining 7 % of variance, the SST structure (f), explaining 7 % and the associated time series (d) with TCC (blue line), SST (red line). The corelation with the TNI Index (green line) is 0.71.

Both TCC structures presented in Fig. 4 are similar with the corresponding TCC structures in ISPCC (Fig. 2) and PATMOS-x (Fig. 3) associated to the EP ENSO and the CP ENSO. This indicates that the ERA5 Reanalysis reproduces fairly well the formation and evolution of total cloud cover on a global scale. The close similarity between the TCC structures derived from satellite observations and reanalysis indicate that the observed results are relevant for the global TCC variability on various time-scales.

### 3.4. Coupled SST-TCC patterns associated to decadal Pacific variability

In order to facilitate the identification of the impact of decadal SST variability on the evolution of global cloud cover, three CCAs were performed between SST and TCC from ISPCC, PATMOS-x and ERA5 Reanalysis, filtered with a 5-year running mean, with the pair of interest from each analysis shown in Fig.5.

All three SST structures (Fig. 5a, b, and c) can be characterized by a horseshoe like structure in the North Pacific with negative anomalies in the north-west surrounded by positive loadings, and an El-Niño like structure in the tropical Pacific. These features have been attributed previously to the positive phase of the Pacific Decadal Oscillation (Mantua et al., 1997; Deser et al., 2010), the Interdecadal Pacific Oscillation (Trenberth and Hurrell, 1994) or the North Pacific Gyre Oscillation (Di Lorenzo et al., 2008). The TCC pattern from the first pair obtained using ISCCP data (Fig. 5a) is dominated by positive anomalies located in the central Tropical Pacific, and negative anomalies extending westward, positively correlated with the SSTs anomalies. Negative anomalies which are anti-correlated with the SSTs anomalies are observed in the north-east and south-east Pacific. These features have been previously associated with Pacific decadal SST variability (Clement et al., 2009). The same characteristics can be observed in the TCC spatial structure obtained using PATMOS-x (Fig. 5h) and ERA5 (Fig. 5i) data, but the negative anomalies are less prominent in the eastern and southern Pacific. The ISCCP - TCC pattern (Fig. 5a) includes positive anomalies over the southern part of North America and the south-eastern part of South America while negative loadings are observed over most of the northern South America and north of Australia. These features were previously associated with positive decadal SST variations in the North Pacific (Garreaud et al., 2009, Newman et al., 2016) and are not captured so well in the pair obtained using the PATMOS-x and ERA5 data. Both the EP ENSO and the CP ENSO project on the evolution of decadal TCC variability in the Pacific basin (Table 1), with the EP ENSO being more prominent. This is in

https://doi.org/10.5194/esd-2021-75
Preprint. Discussion started: 20 October 2021


Earth System Dynamics Discussions
Open Access
EGU

good agreement with previous studies showing that both eastern and central expressions of ENSO are playing significant roles modulating Pacific decadal variability (Di Lorenzo et al., 2010; Furtado et al., 2012).

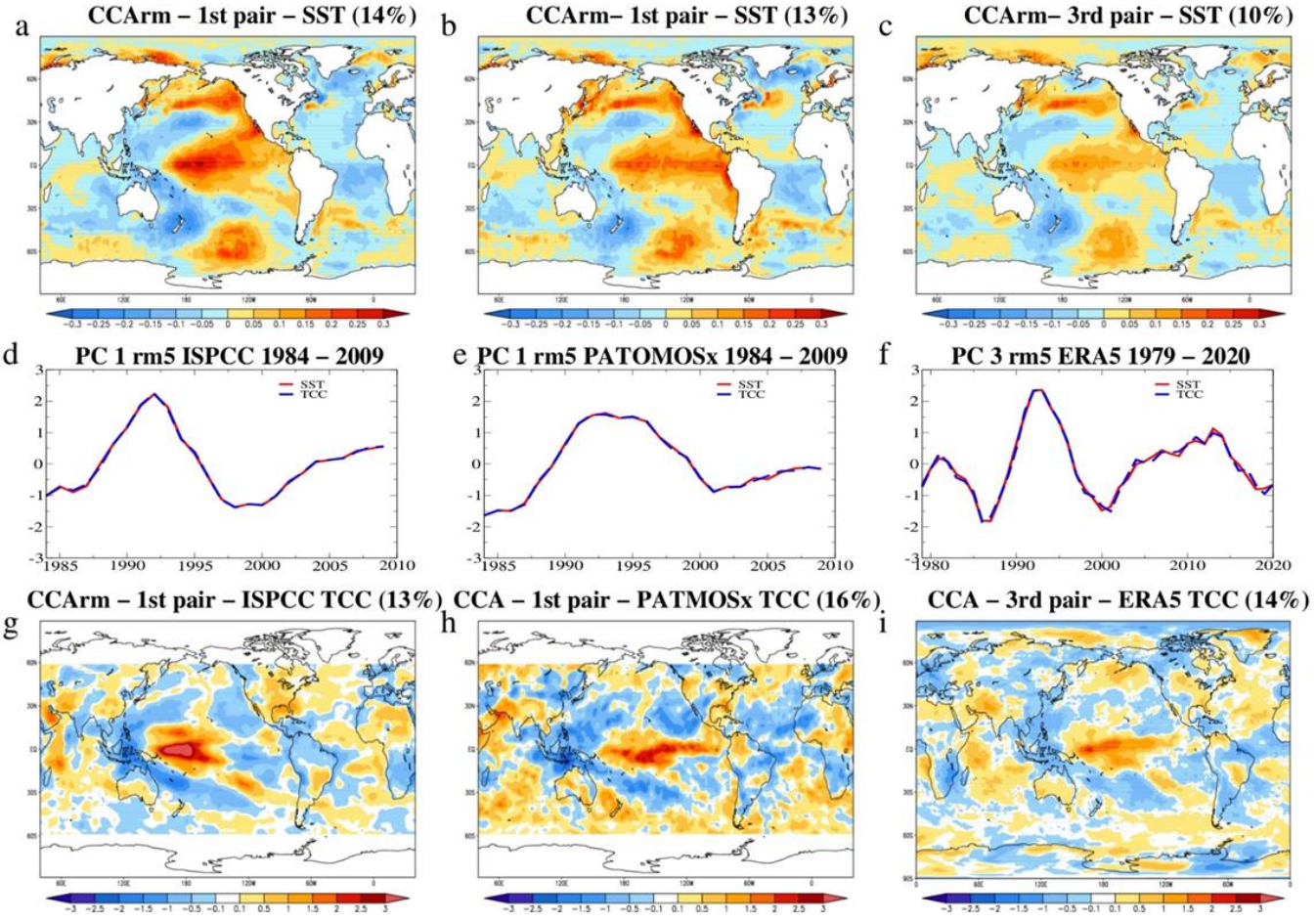


**Figure 5:** Pacific decadal SST variability footprint on global SST-TCC fields identified through CCA using ISPCC, PATMOS-x, and ERA5 total cloud cover data filtered with a 5yr mean. Left column: The first coupled TCC (%) – SST (°C) pair identified through CCA using ISPCC TCC data: the SST pattern (a), explaining 14% of variance, the TCC structure (g), explaining 13% and the associated time series (d) with TCC (blue line), SST (red line). Mid column: The first coupled TCC (%) – SST (°C) pair identified through CCA using PATMOS-x TCC data: the SST pattern (b), explaining 13% of variance, the TCC structure (h), explaining 16% and the associated time series (e) with TCC (blue line), SST (red line). Right column: The third coupled TCC (%) – SST (°C) pair identified through CCA using ERA5 TCC data: the SST pattern (c), explaining 10% of variance, the TCC structure (f), explaining 14% and the associated time series (i) with TCC (blue line), SST (red line).

https://doi.org/10.5194/esd-2021-75
Preprint. Discussion started: 20 October 2021


Earth System Dynamics Discussions
Open Access
EGU

### 3.5 Associated physical processes

In order to investigate the physical mechanisms linking the SST-TCC anomalies and to test the robustness of the EP ENSO and the CP ENSO footprints identified through CCA, we regressed the sea level pressure (SLP), 10m-Wind and total precipitation rate (TPR) fields on the time components (PCs) associated through CCAs with the CP ENSO (Fig. 3c), the EP ENSO (Fig. 3d) and the pacific decadal variability (Fig. 5d), with the results shown in Fig. 6. The regression analysis is restricted to the Tropical Pacific (30°S-30°N) for the first two ENSO modes, and to the North Pacific (0°–60°N) for the maps associated with the decadal variability. The highlighted areas correspond to a statistical significance level above 95%. Similar results are obtained for the PCs derived through CCAs using the PATMOS-x and the ERA5 Reanalysis TCC data (not shown). The regression map of the SLP field on the time component derived through CCA associated with the EP ENSO (Fig. 6a) is dominated by the Southern Oscillation dipole, which is the atmospheric component of a typical El-Nino event (Philander, 1990). The associated TPR structure (Fig. 6b) presents positive anomalies from the eastern to the central tropical Pacific and negative loadings near Indonesia, regions where the most intense TCC anomalies from the CCA pair linked to this mode are located (Fig. 3e). The 10m-Wind (Fig. 6c) is convergent in the warm SST region which, together with the SLP and TPR structure, is consistent with changes in the Walker Circulation associated with the EP ENSO (Bjerknes, 1969; Wang et al., 2016). Unlike the EP ENSO, which includes variations in thermocline, the CP ENSO is a more local air–sea coupling phenomenon located mainly in the central tropical Pacific, which interacts more with Hadley Circulation and is not dependent of changes in the thermocline circulation (Hu et al., 2012).

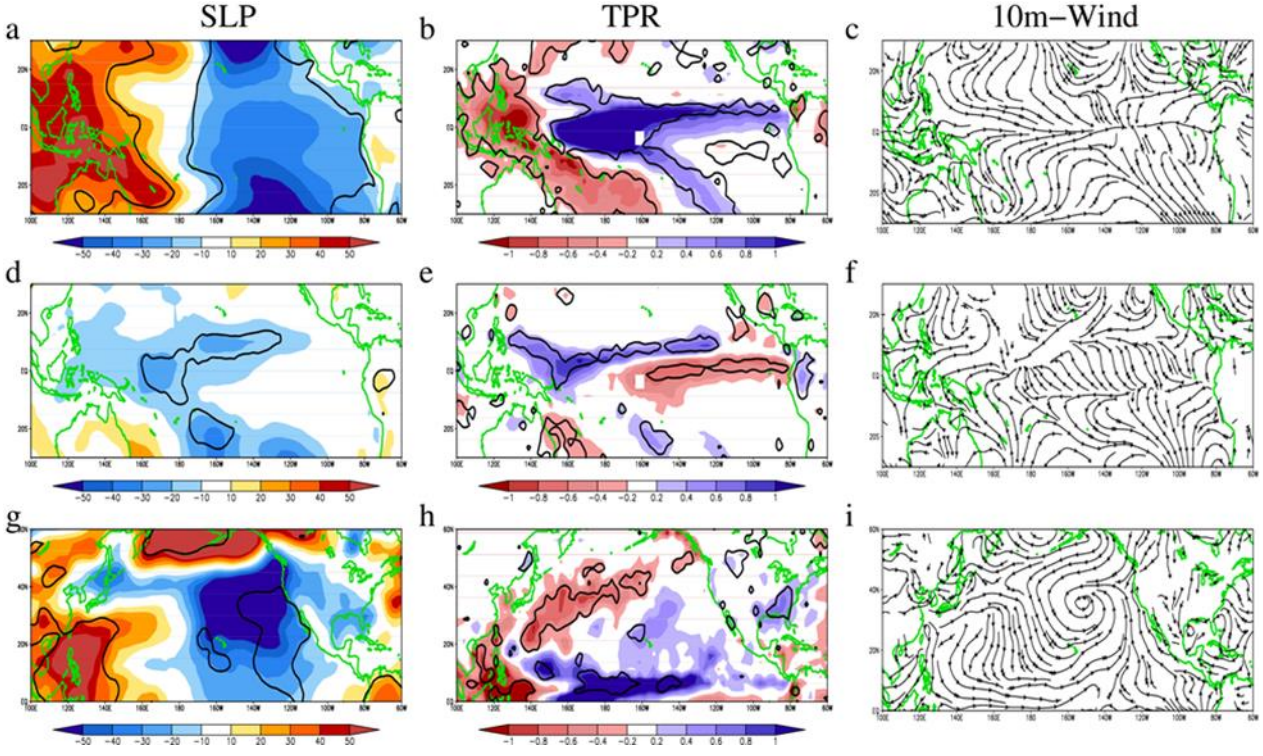

https://doi.org/10.5194/esd-2021-75
Preprint. Discussion started: 20 October 2021


Earth System Dynamics Discussions

**Figure 6:** The regression maps of SLP (%/ hPa) (left, a, d, g), TPR (%/mm/day) (middle, b, e, h) and 10m-Wind (streamline) (right, c, f, i) fields on the time series of CCA pairs associated to: EP ENSO (top row), CP ENSO (middle row) and decadal variability (bottom row) extending over 1984 -2009 period. The associated statistical significance in the highlighted areas is above 95 %.

The SLP regression map (Fig. 6d) associated with CP-ENSO, is dominated by a negative V-like structure starting from central-western Pacific and extending in the subtropics, where the positive SST anomalies from the CCA pair associated with the CP ENSO are located (Fig. 3b). The TPR regression map (Fig. 6e) has a dipole in Central Pacific with the most intense positive values in central-western Pacific, where positive TCC anomalies from the pair associated with the CP ENSO located Fig. 3f). These changes in TPR are related to variations of the intertropical convergence zone (ITCZ) position, generated by CP ENSO (Yu and Kao, 2010). The TPR regression map (Fig. 6h) of the PC from the CCA pair associated with decadal variability (Fig .6d) has positive values in the tropical band, where the positive areas of SST (Fig. 5a) and TCC (Fig. 5g) are located. Negative anomalies are seen in the western extra-tropical Pacific, coincident with negative loadings of SST and TCC. In the western extra-tropical Pacific, where a decrease in ocean temperature and cloudiness was identified (Fig. 5g), negative TPR anomalies are recorded. The SLP regression map associated with decadal variability (Fig. 6g) is dominated by negative anomalies in the subtropical North Pacific and positive anomalies over Alaska and around Indonesia. These features, together with the precipitation and 10m-Wind spatial structures have been previously associated to decadal variations in the Pacific basin (Mantua et al., 1997; Di Lorenzo et al., 2010).

The 10m-Wind, TPR and SLP structures associated with the CP ENSO (Fig. 6d, e, and f) are totally distinct from those associated with the EP ENSO (Fig. 6a, b, and c) and are in good agreement with previous studies investigating the impact of CP ENSO on these fields. Of specific importance is the distinct relation between SST and TCC anomalies, in the tropics and in subtropics. In the deep tropics and in some areas in the subtropics, there is a positive correlation between the SST and TCC anomalies for both modes. This reflects a positive feedback in which relatively warm surface waters increase convection and clouds formation, mainly at high atmospheric levels (Arking and Ziskin, 1994; Back and Bretherton, 2009). In turn, high clouds increase the temperature in the levels below through longwaves absorption and further contribute to the warming of the SSTs, which could lead to an amplification of both ENSO modes (Rädel et al., 2016). In the NE and the SE Pacific, where total cloud cover is dominated by low level marine stratiform clouds, when the SLP is low, positive SSTs are accompanied by negative TCC anomalies. This reflects a distinct feedback, in which reduced cloud cover, associated with weak stability, increase the shortwave radiation fluxes toward ocean surface and result in positive SST anomalies which in turn, reduce low level cloudiness (Clement et al., 2009). This feedback has been confirmed in more recent studies using numerical simulations (Myers and Norris, 2016; Andrews and Webb, 2018) and could extend over the entire planetary ocean, not only in the regions dominated by stratocumulus clouds (Silvers et al., 2017). From this perspective, the persistence of decadal SST anomalies in the NE and SE Pacific is more related to a change in the amount of solar radiation received by the ocean due to a change in cloud cover, than to ocean dynamics, a mechanism also confirmed by Dima and Voiculescu (2016).

https://doi.org/10.5194/esd-2021-75
Preprint. Discussion started: 20 October 2021


Earth System Dynamics Discussions

## 4 Discussion and conclusions

The most important modes of observed and reanalysis global TCC variability, were identified as EOF1 and EOF2 in the global ISPCC, PATMOS-x (1984-2009) and the ERA5 Reanalysis (1979-2020) data. Both EOFs in all three datasets have the most intense values in the Pacific basin and their associated temporal evolution do not present any increasing trend. Together, the two global TCC spatial patterns (EOF 1 + EOF 2) explain two thirds of the total of 45% of variance which can be considered "signal" in the global observed and reanalysis TCC data.

Through a single CCA applied to each of the three TCC datasets, we identify two coupled SST-TCC pairs of spatial structures which were attributed to distinct variations of ENSO, based on their spatial and temporal properties. These associations are also supported by corresponding SLP, 10m-Wind and TPR regression maps on time components from TCC structures identified through CCA. The EP ENSO and the CP ENSO modes are not totally independent from each other, and they can co-exist (Hu et al., 2012; Yu and Kim, 2013). Both, the observed and the reanalysis TCC patterns associated with EP ENSO project strongly on EOF1, while the observed and reanalysis TCC spatial structures associated with the CP ENSO project strongly on EOF2, indicating that the two ENSO modes dominate the evolution of global cloud cover variability. The identification of the EP ENSO and the CP ENSO TCC footprints in the same CCA analysis provides a better perspective regarding the concurrent percentages of global SST and TCC variance explained by these two modes and also allows an estimation of the impact these two modes have on decadal variability. In good agreement with previous investigations, our results suggest that both, the EP ENSO and the CP ENSO, project strongly on Pacific decadal SST and TCC variability. This indicates that, although not perfect, satellite cloud cover data can be used to investigate both the inter-annual and the decadal climate variability.

The Pacific sector in the ISPCC (Fig. 2e and f), the PATMOS-x (Fig. 3e and f) and the ERA5 Reanalysis (Fig. 4e and f) TCC patterns looks almost identical, indicating a robust structure associated with the EP ENSO and the CP ENSO modes, regardless of the data set or the period analysed. Over the continents, the PATMOS-x data captures better the impact of the EP ENSO and the CP ENSO over the North America, South America and Australia, making them more suitable for future regional analyses. Opposing, the ISCCP data seem to be more reliable for identifying decadal Pacific variations. There are many indices that have been proposed and used to identify different ENSO types, based on ocean surface temperature (Ashok et al., 2007; Kug et al., 2009), on ocean salinity (Qu and Yu, 2014) or on outgoing longwave radiation (Chiodi and Harrison, 2015). Our approach, through multivariate statistical analyses, provide two independent continuous ENSO indices based entirely on total cloud cover anomalies.

The positive correlation between the SST and TCC anomalies together with the negative SLP over the tropical Pacific, which is dominated by high clouds, indicate that the TCC anomalies are induced by changes in SST through convection. On the other hand, high clouds could provide positive feedback to SST in these regions through their impact on the radiative transfer (Bony et al., 2015). The negative SST/TCC correlation observed in the NE and the SE Pacific, where total cloud cover is dominated by low level marine stratiform clouds suggests that another positive feedback between clouds and SST exists (Clement et al.,

https://doi.org/10.5194/esd-2021-75
Preprint. Discussion started: 20 October 2021


Earth System Dynamics Discussions

2009). Therefore, the amplitudes of the highest TCC anomalies, which are located in the tropics and in subtropics, appear to be related to these two distinct feedbacks. However, the fact that these feedbacks manifest in the same manner (with regard to the sign of the correlation between SST and TCC anomalies) for both of the ENSO types, indicates that they are not responsible for the different manifestations of the EP ENSO and the CP ENSO modes. A consensus regarding the physical mechanism describing the CP ENSO has not been yet reached, with ocean advection processes (Kug and Ahn, 2009) or changes in equatorial easterly and westerly anomalies (Ashok et al., 2007; Hu et al., 2012) being proposed as the main drivers in generating this phenomenon.

The large amount of cumulative variance explained by the two ENSO modes in the observed and reanalysis global TCC field and their connections with the two positive feedbacks, which can act to amplify the mechanisms of both modes, imply that they are playing a critical role in the global radiative balance, especially in the context of climate change. Such a decomposition of the global total cloud cover field based on a linear combination of coupled SST-TCC pairs (as derived through CCA) and of eigenmodes (derived through EOF analysis) could provide a reference against which one could validate the performance of general circulation models in simulating global cloud cover variability.

**Data availability**

All data sources are mentioned in the Methods section.

**Code availability**

Codes are available from the corresponding author.

**Author contribution**

P.V. initiated this research, performed the analyses and made the figures. All authors participated in discussions during this study and equally contributed to the writing and revising the manuscript.

**Competing interests**

The authors declare that they have no conflict of interest.

https://doi.org/10.5194/esd-2021-75
Preprint. Discussion started: 20 October 2021


Earth System Dynamics Discussions

**Acknowledgments**

This work was supported by The Deutsche Bundesstiftung Umwelt DBU (German Federal Environmental Foundation) through the DBU Alumni Fellowship program. MI is supported by Helmholtz Association through the joint program "Changing Earth - Sustaining our Future" (PoF IV) program of the AWI. Funding by the AWI Strategy Fund Project - PalEX and by the Helmholtz Climate Initiative - REKLIM is gratefully acknowledged. ISCCP and PATMOS-x projects are acknowledged for the cloud data. Corrected ISCCP and PATMOS-x data were provided by the Research Data Archive at NCAR. The HadISST data set was provided by the British Met Office, Hadley Centre. The NINO3 Index, the TNI Index and the $CO_2$ concentration recorded at Mauna Loa Observatory were provided by the NOAA/OAR/ESRL PSD, Boulder, Colorado, USA, from their website at https://www.ncdc.noaa.gov/data-access/marineocean-data/extended-reconstructed-sea-surface-temperature-ersst-v3b and at https:/www.esrl.noaa.gov/psd/gcos_wgsp/Timeseries/. The European Centre For Medium-Range Weather Forecasts (ECMWF) is acknowledged for ERA 5 Reanalysis data.

https://doi.org/10.5194/esd-2021-75
Preprint. Discussion started: 20 October 2021


Earth System Dynamics Discussions

## References

Adler, R. F., Huffman, G. J., Chang, A., Ferraro, R., Xie, P., Janowiak, J., Rudolf, B., Schneider, U., Curtis, S., Bolvin, D., Gruber, A., Susskind, J., Arkin, P., and Nelkin, E.: The Version 2 Global Precipitation Climatology Project (GPCP) Monthly Precipitation Analysis (1979-Present), J Hydrometeor, 4, 1147-1167, https://doi.org/10.1175/1525-7541(2003)004<1147:TVGPCP>2.0.CO;2, 2003.

Alexander, M. A., Blade, I., Newman, M., Lanzante, J. R., Lau, N. C., and Scott, J. D.: The atmospheric bridge: The influence of ENSO teleconnections on air-sea interaction over the global oceans, J Climate, 15 (16), 2205–2231, https://doi:10.1175/1520-0442(2002)015<2205:tabtio>2.0.co;2, 2002.

Andrews, T. and Webb, M. J.: The dependence of global cloud and lapse-rate feedbacks on the spatial structure of tropical Pacific warming, J Climate, 31(2), 641–654, https://doi.org/10.1175/JCLI-D-17-0087.1, 2018.

Arking, A. and Ziskin, D.: Relationship between clouds and sea surface temperatures in the western201 tropical Pacific, J Climate, 7, 988–1000, https://doi: 10.1175/1520-0442(1994)007<0988:RBCASS>2.0.CO;2, 1994.

Ashok, K., Behera, S., Rao, A. S., Weng, H. Y., and Yamagata, T.: El Niño Modoki and its teleconnection, J Geophys Res, 112, https://doi.org/10.1029/2006JC003798, 2007.

Ashok, K., Tam, C. Y., and Lee, W. J.: ENSO Modoki impact on the Southern Hemisphere storm track activity during extended austral winter, Geophys Res Lett, 36, 12, https://doi.org/10.1029/2009GL038847, 2009.

Ashok, H. and Yamagata, T.: Climate change: The El Niño with a difference, Nature, 461, 481–484, https://doi:10.1038/461481a, 2009.

Back, L. E. and Bretherton, C. S.: A simple model of climatological rainfall and vertical motion232 patterns over the tropical oceans, J Climate, 22, 6477–6497, 2009.

Bjerknes, J.: Atmospheric teleconnections from the equatorial Pacific, Mon Weather Rev, 97, 163–172, https://doi.org/10.1175/1520-0493(1969)097<0163:ATFTEP>2.3.CO;2, 1969.

Bony, S., Dufresne, J.-L., Le Treut, H., Morcrette, J.-J., and Senior, C.: On dynamic and thermodynamic components of cloud changes, Clim Dynam, 22, 71–86, https://doi:10.1007/s00382-003-0369-6, 2004.

Bony, S., Stevens, B., Frierson, D. M. W., Jakob. C., Kageyama, M., Pincus, R., Shepherd, T. G., Sherwood, S. C., Siebesma, A. P., Sobel, A. H., Watanabe, M. and Webb, M. J.: Clouds, circulation and climate sensitivity, Nat Geosci, 8, 261–268, http://doi:10.1038/NGEO23, 2015.

Bretherton, C. S., Widmann, M., Dymnikov, V. P., Wallace, J. M. and Blade, I.: The effective number of spatial degrees of freedom of a time-varying field, J Climate, 12, 1990–2009, 1999.

https://doi.org/10.5194/esd-2021-75
Preprint. Discussion started: 20 October 2021


Berrisford, P., Dee, D. P., Poli, P., Brugge, R., Fielding, K., Fuentes, M., Kållberg, P. W., Kobayashi, S., Uppala, S., and Simmons, A.: The ERA-Interim archive Version 2.0. ERA Report Series 1, 2011.

Campbell G. G. and Holmlund, K..: Geometric cloud heights from Meteosat, International Journal of Remote Sensing, 25:21, 4505-4519, DOI: 10.1080/01431160410001726076, 2004

Cess, R., Potter, G. L., Blanchet, J. P., Boer, G. J., Del Genio, A. D., Déqué, M., Lacis, A. A., Le Treut, H., Li , Z. -x., Liang, X. -z., Mcavaney, B. J., Randall, D. A., Rikus, T. L., Roeckner, Ø E., and Royer, J. F.: Intercomparison and interpretation of climate feedback processes in 19 atmospheric general circulation models, J Geophys Res, 95, 16.601–16.615, https://doi.org/10.1029/JD095iD10p16601, 1990.

Chiodi, A. M. and Harrison, D. E.: El Niño impacts on seasonal US atmospheric circulation, temperature, and precipitation anomalies: the OLR-event perspective, J Climate, 26, 822–37, https://doi.org/10.1175/JCLI-D-14-00387.1, 2013.

Chiodi, A.M. and D.E. Harrison, .: Global Seasonal Precipitation Anomalies Robustly Associated with El Niño and La Niña Events—An OLR Perspective, J Climate, 28, 6133–6159, https://doi.org/10.1175/JCLI-D-14-00387.1, 2015.

Clement, A. C., Burgman, R. and Norris, J. R.: Observational and Model Evidence for Positive Low-Level Cloud Feedback, Science, 325, 460-464, https://doi.org/10.1126/science.1171255, 2009.

Deser, C., Alexander, M. A., Xie, S. P., and Phillips, A. S.: Sea surface temperature variability: patterns and mechanisms, Annu Rev Mar Sci, 2, 115–143, https://doi.org/10.1146/annurev-marine-120408-151453, 2010.

Di Lorenzo, E., Schneider, N., Cobb, K., Franks, P., Chhak, K., Miller, A., Mcwilliams, J., Bograd, S., Arango, H., Curchitser, E., Powell, T., and Rivière, P.: North Pacific Gyre Oscillation links ocean climate and ecosystem change, Geophys Res Lett, 35, L08607, https://doi.org/10.1029/2007GL032838, 2008.

Di Lorenzo, E., Cobb, K. M., Furtado, J. C., Schneider, N., Anderson, B. T., Bracco, A., Alexander, M. A., and Vimont, D. J.: Central Pacific El Niño and decadal climate change in the North Pacific Ocean, Nat Geosci, 3, 762–765, https://doi.org/10.1038/ngeo984, 2010.

Dima, M. and Voiculescu, M.: Global patterns of solar influence on high cloud cover, Clim Dynam, 1432-0894, https://doi.org/10.1002/2016GL069961, 2016.

Dufresne, J. L. and Bony, S.: An assessment of the primary sources of spread of global warming estimates from coupled atmosphere–ocean models, J Climate, 21, 5135–5144, https://doi.org/10.1175/2008JCLI2239.1, 2008.

Evan, A. T., Heidinger, A. K., and Vimont, D. J.: Arguments against a physical long-term trend in global ISCCP cloud amounts, Geophys Res Lett, 34, L04701, https://doi.org/10.1029/2006GL028083, 2007.

Feng, J. and Li, J.: Influence of El Niño Modoki on spring rainfall over South China, J Geophys Rese, 116, D13, https://doi.org/10.1029/2010JD015160, 2011.

https://doi.org/10.5194/esd-2021-75
Preprint. Discussion started: 20 October 2021


Freund, M.B., Henley, B.J., Karoly, D.J., McGregor, H.V., Abram, N. J., Dommenget, D.: Higher frequency of Central Pacific El Niño events in recent decades relative to past centuries. Nat. Geosci. 12, 450–455 https://doi.org/10.1038/s41561-019-0353-3, 2019

Furtado, J. C., Di Lorenzo, E., Anderson, B. T., and Schneider, N.: Linkages between the North Pacific Oscillation and central tropical Pacific SSTs at low frequencies, Clim Dynam, 39, 2833–2846, https://doi.org:10.1007/s00382-011-1245-4, 2012.

Hersbach, H., Bell, B., Berrisford, P., Hirahara, S., Horányi, A., Muñoz-Sabater, J., Nicolas, J., Peubey C, Radu, R., Schepers, D., Simmons, A., Soci, C., Abdalla, S., Abellan, X., Balsamo G., Bechtold, P., Biavati, G, Bidlot, J., Bonavita, M., De Chiar, G., Dahlgren, P., Dee, D., Diamantakis, M., Dragani, R., Flemming, J., Forbes, R., Fuentes, M., Geer, A., Haimberger, L., Healy, S., Hogan, R. J., Hólm, E., Janisková, M., Keeley, S., Laloyaux, P., Lopez, P., Lupu, C., Radnoti, G., de Rosnay, P., Rozum, I., Vamborg, F., Villaume, S., and Thépaut, J. N.: The ERA5 global reanalysis, Q J Roy Meteor Soc, 146 (730), 1999–2049, https://doi.org/10.1002/qj.3803, 2020.

Heidinger, A. K., Foster, M. J., Walther A., and Zhao, X.: The Pathfinder Atmospheres–Extended (PATMOS-x) AVHRR climate dataset, B Am Mereorol Soc, 95, 909–922, https://doi.org/10.1175/BAMS-D-12-00246.1, 2014.

Heidinger, A. K., Evan, A. T., Foster, M. J., and Walther A.: A naive Bayesian cloud detection scheme derived from CALIPSO and applied to PATMOS-x, J Appl Meteorol Clim, 51, 1129– 1144, https://doi.org:10.1175/JAMC-D-11-02.1, 2012.

Hu, Z. Z., Kumar, A., Jha, B., Wang, W., and Huang, B.: An analysis of warm pool and cold tongue El Niños: Air-sea coupling processes, global influences, and recent trends, Clim Dynam, 38, https://doi.org/10.1007/s00382-011-1224-9, 2012.

Jacobowitz, H., Stowe, L. L., Ohring, G., Heidinger, A., Knapp, K., and Nalli, N. R.: The Advanced Very High Resolution Radiometer Pathfinder Atmosphere (PATMOS) climate data set: A resource for climate research, B Am Meteorol Soc, 84, 785–793, https://doi.org/10.1175/BAMS-84-6-785, 2003.

Jeong, H. and Ahn, J.: A new method to classify ENSO events into eastern and central Pacific types, Int J Climatol, 37, 2193-2199, https://doi.org/10.1002/joc.4813, 2016.

Kao, H.Y. and Yu, J. Y.: Contrasting eastern-Pacific and central-Pacific types of ENSO, J Climate, 22, 615–632, https://doi.org/10.1175/2008JCLI2309.1, 2009.

Klein, S. A., Zhang, Y., Zelinka, M. D., Pincus, R., Boyle, J., and Gleckler, P. J.: Are climate model simulations of clouds improving? An evaluation using the ISCCP simulator, Journal of Geophysical Research: Atmospheres, 118, 1329–1342. https://doi.org/10.1002/jgrd.50141, 2013.

https://doi.org/10.5194/esd-2021-75
Preprint. Discussion started: 20 October 2021


Kug, J. S., Jin, F.F., and Ahn, S. I.: Two types of El Niño events: cold tongue El Nino and warm pool El Niño, J Climate, 22, 1499–1515, https://doi.org/10.1175/2008JCLI2624.1, 2009.

Larkin, N. K. and Harrison, D. E.: Global seasonal temperature and precipitation anomalies during El Niño autumn and winter, Geophys Res Lett, 32 (L16705), https://doi.org/10.1029/2005GL022860, 2005.

Lorenz, E. N.: Empirical orthogonal functions and statistical weather prediction, Technical Report 1, Statistical Forecasting Project, 48 pp., Department of Meteorology, MIT, Cambridge, 1956.

Mantua, N. J., Zhang, Y., Wallace, J. M., and Francis, R. C.: A Pacific interdecadal climate oscillation with impacts on salmon production, B Am Meteorol Soc, 78, 1069–1079, https://doi.org/10.1175/1520-0477(1997)078<1069:APICOW>2.0.CO;2, 1997.

Marsh, N. and Svensmark, H.: Galactic cosmic ray and El Nin˜o—Southern Oscillation trends in International Satellite Cloud Climatology Project D2 low-cloud properties, J Geophys Res, 108, D6, https://doi.org/10.1029/2001JD001264, 2003.

McPhaden, E., Zebiak,W., and Glantz, M. H.: ENSO as an intriguing concept in Earth science. Science, 314, 1740–1745, https://doi.org/10.1126/ science.1132588, 2006.

Myers, T. A. and Norris, J. R.: Reducing the uncertainty in subtropical cloud feedback, Geophys Res Lett, 43, 2144–2148, https://doi.org/10.1002/2015GL067416, 2016.

Newman, M., Alexader, M. A., Ault, T. R., Cobb, K. M., Deser, C., Di Lorenzo, E., Mantua, N. J., Miller, A. J., Minobe, S., Nakamura, H., Schneider, N., Vimont, D. J., Phillips, A. S., Scott, J.D., and Smith, C.A: The Pacific Decadal Oscillation, Revisited, J Climate 29, 4399–4427, https://doi.org/10.1175/JCLI-D-15-0508.1, 2016.

Norris, J. R.: Multidecadal changes in near-global cloud cover and estimated cloud cover radiative forcing. J Geophys Res, 110, D08206, doi:10.1029/2004JD005600, 2005

Norris, J. R., and Slingo, A.: Trends in observed cloudiness and Earth's radiation budget: What do we not know and what do we need to know? Clouds in the Perturbed Climate System: Their Relationship to Energy Balance, Atmospheric Dynamics, and Precipitation, J. Heintzenberg and R. J. Charlson, Eds., Strüngmann Forum Reports, MIT Press, 17–36, DOI:10.7551/mitpress/9780262012874.003.0002, 2009.

Norris, J. R. and Evan, A. T.: Empirical removal of artifacts from the isccp and patmos-x satellite cloud records, J Atmos Ocean Tech, 32, 691–702, https://doi.org/10.1175/JTECH-D-14-00058.1, 2015.

Pallé, E.: Possible satellite perspective effects on the reported correlations between solar activity and clouds, Geophys Res Lett, 32(3), L03802, 2005.

Philander, S.G.H.: El Nino, La Nina, and the Southern Oscillation (pp. 293) Academic Press, Waltha, https://doi.org/10.1126/science.248.4957.904, 1990.


Qu, T. and Yu, J.-Y.: ENSO indices from sea surface salinity observed by Aquarius and Argo, J Oceanogr, 70, 367–375, doi:10.1007/s10872-014-0238-4, 2014.

Rädel, G., Mauritsen, T., Stevens, B., Dommenget, D., Matei, D., Bellomo, K., and Clement, A.: Amplification of El Niño by cloud longwave coupling to atmospheric circulation, Nat Geosci, 9, 106–110, doi:10.1038/ngeo2630, 2016.

Ramanathan, V., Cesss, R. D., Harrison, E. F., Minnis, P., Barkstrom, B. R., Ahmad, E., and Hartmann, D.: Cloud-radiative forcing and climate: results from the Earth Radiation Budget Experiment, Science, 243, 57–63, 1989.

Ramanathan, V., and Collins, W.: Thermodynamic regulation of ocean warming by cirrus clouds239 deduced from observations of the 1987 El Nino, Nature, 351, 27–32, https://doi.org/10.1038/351027a0, 1991.

Rasmusson, E. M. and Carpenter, T. H.: Variations in tropical sea surface temperature and surface wind fields associated with the Southern Oscillation/El Ni˜no, Mon Weather Rev, 110, 354–384, https://doi.org/10.1175/1520-0493(1982)110<0354:VITSST>2.0.CO;2, 1982.

Rayner, N. A., Parker, D. E., Horton, E. B., Folland, C. K., Alexander, L. V., and Rowell, D. P.: Global analyses of sea surface temperature, sea ice, and night marine air temperature since the late nineteenth century, Journal of Geophysical Research, 108., https://doi.org/10.1029/2002JD002670, 2003.

Ren, H.-L. and Jin, F.-F.: Niño indices for two types of ENSO, Geophys Res Lett, 38, https://doi.org/10.1029/2010GL046031, 2011.

Rossow, W. B., Walker, A. W., Beuschel, D. E., and Roiter, M. D.: International Satellite Cloud Climatology Project (ISCCP): Documentation of new cloud datasets. WMO Tech. Doc. WMO/ TD-737, 115 pp. [Available online at http://isccp.giss.nasa.gov/ pub/documents/d-doc.pdf.], 1996.

Rossow, W. B., and Schiffer, R. A.: Advances in understanding clouds from ISCCP, B Am Mereorol Soc, 80, 2261–2287, doi:10.1175/1520-0477(1999)080<2261:AIUCFI>2.0.CO;2, 1999.

Silvers, L. G., Paynter, D., and Zhao, M.: The diversity of cloud responses to twentieth century sea surface temperatures, Geophys Res Lett, 45, 391–400, https://doi.org/10.1002/2017GL075583, 2017.

Timmermann, A., An, S.-I., Kug, J.-S., Jin, F.-F., Cai, W., Capotondi, A., Cobb, K., Lengaigne, M., McPhaden, M. J., Stuecker, M. F., Stein, K., Wittenberg, A. T., Yun, K.-S., Bayr, T., Chen, H.-C., Chikamoto, Y., Dewitte, B., Dommenget, D., Grothe, P., Guilyardi, E., Ham, Y.-G., Hayashi, M., Ineson, S., Kang, D., Kim, S., Kim, W., Lee, J.-Y., Li, T., Luo, J.-J., McGregor, S., Planton, Y., Power, S., Rashid, H., Ren, H.-L., Santoso, A., Takahashi, K., Todd, A., Wang, G., Wang, G., Xie, R., Yang, W.-H., Yeh, S.-W., Yoon, J., Zeller, E., and Zhang, X.: El Niño–Southern Oscillation complexity. Nature, 559 (7715), 535– 545, https://doi.org/10.1038/s41586-018-0252-6, 2018.


Trenberth, K. E. and Hurrell, J.W.: Decadal atmosphere-ocean variations in the Pacific, Clim Dynam, 9, 303-319, https://doi.org/10.2151/jmsj1965.75.3_657, 1994.

Trenberth, K. E. and Stepaniak, D. P.: Indices of El Ni˜no evolution, J Climate, 14, 1697–1701, https://doi.org/10.1175/1520-0442(2001)014<1697:LIOENO>2.0.CO;2, 2001.

Vaideanu, P., Dima, M., and Voiculescu, M.: Atlantic Multidecadal Oscillation footprint on global high cloud cover. Theor Appl Climatol, https://doi.org/10.1007/s00704-017-2330-3, 2017.

von Storch, H. V. and Zwiers, F. W.: Statistical Analysis in Climate Research, Cambridge University Press, (484 pp), https://doi.org/10.1002/1097-0088(20000615)20:7<811::AID-JOC510>3.0.CO;2-P, 1999.

Wang, C., Deser, C., Yu, J.-Y., DiNezio, P., and Clement, A.: El Niño-Southern Oscillation (ENSO): A review. In Coral Reefs of the Eastern Pacific, P. Glymn, D. Manzello, and I. Enochs, Eds., Springer Science Publisher, 85-106, 2016.

Yeh, S.-W., Kug, J.-S., Dewitte, B., Kwon, M.-H., Kirtman, B., Jin, F.-F.: El Niño in a changing climate, Nature, 461, 511–514, https://doi.org/10.1038/nature08316, 2009.

Yeh, S.-W., Cai, W., Min, S.-K., McPhaden, M. J., Dommenget, D., Dewitte, B., Collins, M., Ashok, K., An, S.-I.,Yim, B.-Y., Kug, J.-S.: ENSO atmospheric teleconnections and their response to greenhouse gas forcing, Rev Geophy, 56, 185– 206, https://doi.org/10.1002/2017RG000568, 2018.

Yu, J.-Y., Kao, H.-Y., Lee, T.: Subtropics-related interannual sea surface temperature variability in the equatorial central Pacific, J Climate, 23, 2869–2884, https://doi.org/10.1175/2010JCLI3171.1, 2010.

Yu, J-Y. and Kim, S. T.: Identifying the types of major El Niño events since 1870, Int J Climatol, 33, 2105-2112. https://doi.org/10.1002/joc.3575, 2013.

Zelinka, M. D. and Hartmann, D. L.: The observed sensitivity of high clouds to mean surface temperature anomalies in the tropics, J Geophys Res, doi: 10.1029/2011JD016459, 2011.

Zelinka, M.D., Grise, K. M., Klein, S. A., Zhou, C., DeAngelis, A. M., and Christensen, M.W.: Drivers of the Low-Cloud Response to Poleward Jet Shifts in the North Pacific in Observations and Models, J Climate, 31, 7925–7947, https://doi.org/10.1175/JCLI-D-18-0114.1, 2018.

Zhou, C., Zelinka, M. D., and Klein, S. A.: Impact of decadal cloud variations on the Earth's energy budget, Nat Geosci, 9, 871–874, https://doi.org/10.1038/ngeo2828, 2016.